A Study of Microstrip Array Antennas with the Feed Network

ELY LEVINE, MEMBER, IEEE, GABI MALAMUD, SHMUEL SHTRIKMAN, FELLOW, IEEE, AND DAVID TREVES, FELLOW, IEEE

Abstract—**The radiation and losses in microstrip antennas with a corporate feed network are studied. First, we apply a surface current approach in which the electrical currents in the feed lines are modeled as in ideal transmission lines. The free space radiation and the surface wave excitation of typical segments in printed feed networks are studied. A four-element array antenna with its printed feed network is analyzed and predicted radiation patterns, directivity, and gain are presented and compared with experimental results. The gain and directivity of large arrays of 16, 64, 256 and 1024 elements are calculated and measurements in the frequency range of 10 to 35 GHz are reported.**

I. Introduction

PRINTED ANTENNAS ARE promising candidates for microwave and millimeter wave applications, where the weight and the volume of the antenna should be kept to a minimum, or when conformal arrays are needed. However, printed arrays show low efficiency due to ohmic and dielectric losses in the feed network, due to parasitic radiation in the feed network, and due to the excitation of surface waves in the dielectric substrate [1]–[3]. The efficiency limitations are most severe in large arrays where the feed network is long and complicated, and at high frequencies (K or Ka bands) where the dielectric and ohmic losses are high. In recent years, several high-gain printed arrays were investigated [4], [5], especially for direct broadcast satellite (DBS) applications [6]–[8].

The purpose of this work is to present an analysis of the radiation and the losses of microstrip arrays including the feed network effects. The discussion is restricted to single-layer microstrip arrays built on commercial substrates with dielectric constants close to two. This analysis can give useful estimations of the available gains in various arrays, and also provides a theoretical prediction of the radiation patterns in the presence of feed lines. There are only a very few publications on such network effects [9], [10], mainly because solutions based on moment methods or on conjugate gradient methods require a vast amount of computation, and therefore are not very practical for general design purposes. A recent contribution [11] based on a magnetic current model gives a detailed assessment of the feed network effects.

Our approach is based on a surface current model [12] in which the printed radiators and the feed lines are replaced by assumed current distributions. The currents in the radiating elements are derived from cavity or equivalent transmission-line models and the currents in the feed lines are taken as traveling waves. The radiation fields and the surface-wave excitation are then found from the assumed currents using the appropriate Green's function in the Fourier domain. The ohmic and dielectric losses in the feed lines are calculated using known formulas from the literature [13]–[15].

In Section II, the mechanism of radiation and surface wave excitation emerging from typical microstrip segments is briefly reviewed. In Section III, an analysis of four element arrays, including the feed network, is presented and compared to results without the network. Experimental results of several four element arrays are also given. The directivity and the gain of modular designed arrays [16], [17] are studied in Section IV, and compared to experimental results of 16, 64, 256 and 1024 element arrays, built for frequencies of 10, 20, 30 and 35 GHz, respectively. These results can be used as a general estimation of the gain limitations in large printed arrays.

II. Radiation and Losses in Microstrip Lines

We consider a planar microstrip configuration with an infinite metallic ground plane at $z = 0$ and a planar dielectric substrate of height h and dielectric constant ϵ_r. We are interested in the electromagnetic fields due to any arbitrary current distribution $\bar{J}(x, y)$. Following the surface current analysis in the spectral domain described in [12] one can represent the current distribution by its Fourier decomposition:

$$\bar{J}(x,y) = \frac{1}{4\pi^2}\int\int_{-\infty}^{+\infty} \tilde{\bar{J}}(k_x,k_y)e^{-j(k_x x+k_y y)}\,dk_x dk_y \quad (1)$$

where the tilde over a variable denotes its Fourier transform, and $j = \sqrt{-1}$. The same transformation is done for $\bar{E}$ and $\bar{H}$. The electric fields and the surface currents are related by

$$\tilde{E}_i(k_x,k_y) = \tilde{G}_{ij}(k_x,k_y)\tilde{J}_j(k_x,k_y), \qquad i,\ j = x,y \quad (2)$$

where the matrix $\tilde{G}$ is the dyadic Green's function for an elemental surface current source in the Fourier domain.

The complex input power into the antenna is

$$P_{\text{in}} = -\frac{1}{2}\int\int_{-\infty}^{+\infty} \tilde{\bar{E}}(k_x,k_y)\cdot\tilde{\bar{J}}^*(k_x,k_y)\,dk_x dk_y. \quad (3)$$

The contribution due to radiation into free space comes from the "visible range" in which $k_x^2 + k_y^2 < k_0^2$. Transforming to spherical coordinates by $k_x = k_0 \sin\theta\cos\phi$ and $k_y = k_0 \sin\theta \sin\phi$ and integrating over a sphere of radius k_0, the

Manuscript received April 24, 1987; revised November 10, 1987.

E. Levine is with Elta Electronics Industries Ltd., Ashdod 77102, Israel.
G. Malamud, S. Shtrikman, and D. Treves are with the Department of Electronics, Weizmann Institute of Science, Rehovot 76100, Israel.

IEEE Log Number 8825323.

power radiated into free space is given by

$$P_r = \int_0^{\pi/2} \int_0^{2\pi} f(\theta, \phi) \sin\theta d\theta d\phi \tag{4}$$

where

$$f(\theta,\phi) = \frac{15k_0^2}{\pi} \cdot \left(\frac{|-\tilde{J}_x \sin\phi + \tilde{J}_y \cos\phi|^2 \cos^2\theta}{(\epsilon_r - \sin^2\theta)\cot^2(hk_0\sqrt{\epsilon_r - \sin^2\theta}) + \cos^2\theta} + \frac{|\tilde{J}_x \cos\phi + \tilde{J}_y \sin\phi|^2 \cos^2\theta(\epsilon_r - \sin^2\theta)}{(\epsilon_r - \sin^2\theta) + \epsilon_r^2 \cos^2\theta \cot^2(hk_0\sqrt{\epsilon_r - \sin^2\theta})} \right). \tag{5}$$

The expression for $f(\theta, \phi)$ is the free space radiation power pattern.

When we examine values of $k_t^2 = k_x^2 + k_y^2$ which are greater than k_0^2 (the "invisible range"), we find that the power propagated by surface waves in the first transverse magnetic (TM) mode is given by

$$P_s = \int_0^{2\pi} f_s(k_{tp}, \phi)\, d\phi \tag{6}$$

where

$$f_s(k_{tp},\phi) = A_s 15k_0^2 |\tilde{J}_x(k_{tp},\phi)\cos\phi + \tilde{J}_y(k_{tp},\phi)\sin\phi|^2 \tag{7}$$

and

$$A_s = \frac{\epsilon_r(x_p^2 - 1)x_p}{\epsilon_r x_p \left(\frac{1}{\sqrt{x_p^2 - 1}} - \frac{\sqrt{x_p^2 - 1}}{x_p^2 - \epsilon_r} \right) + x_p k_0 h \left(1 + \frac{\epsilon_r^2(x_p^2 - 1)}{\epsilon_r - x_p^2} \right)}$$

$$x_p \equiv \frac{k_{tp}}{k_0}$$

$$k_{tp}^2 = k_x^2 + k_y^2$$

is the first solution of

$$j\epsilon_r\sqrt{k_0^2 - k_{tp}^2}\cot(\sqrt{\epsilon_r k_0^2 - k_{tp}^2}h) - \sqrt{\epsilon_r k_0^2 - k_{tp}^2} = 0$$

and k_x, k_y have been transformed to cylindrical coordinates by

$$k_x = k_{tp}\cos\phi; \quad k_y = k_{tp}\sin\phi.$$

The integrand in (6) represents a one-dimensional "radiation pattern," where ϕ is the "angle of radiation" with respect to the $\hat{x}$ axis. Additional aspects of this model, more details about the calculations, and numerical results can be found in [12].

Now consider a microstrip line printed on a grounded dielectric substrate of thickness h and dielectric constant ϵ_r where the width and length of the line are W_l and L, respectively (Fig. 1). The two cases of end-fed and center-fed lines shown in this figure are the most typical building blocks in antenna feed networks. At this stage the printed lines are regarded as lossless transmission lines, e.g., the current along the line is not influenced by the dielectric, ohmic, and radiative losses. The effective dielectric constant and the characteristic impedance of the line are [18]

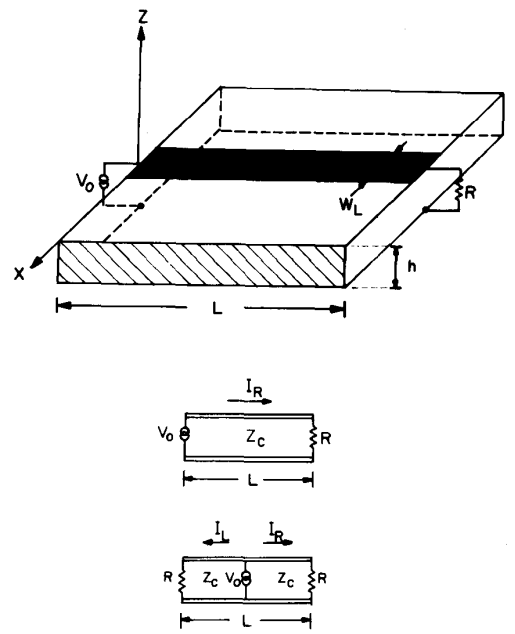

Fig. 1. A microstripline geometry. (a) The structure and the dimensions of an end-fed microstripline. (b) Two schematic feeds: end-fed and center-fed. In both cases the lines are matched in their ends.

$$\epsilon_{\text{eff}} = \frac{\epsilon_r + 1}{2} + \frac{\epsilon_r - 1}{2\sqrt{1 + 10\frac{h}{W_l}}} \tag{8}$$

$$Z_c = \frac{120\pi h}{\sqrt{\epsilon_{\text{eff}}}} \cdot \begin{cases} [W_l + 2.42h - 0.44h^2/W_l + h(1 - h/W_l)^6]^{-1}, & \text{if } h \le W_l \\ \ln(8h/W_l + W_l/4h)/2\pi h, & \text{if } h \ge W_l. \end{cases} \tag{9}$$

The current and voltage in a transmission line which is fed at its end by the voltage $V_0 e^{j\omega t}$ and loaded by the resistance R at its other side are [19]

$$V(y) = V_0(e^{-j\beta y} + \Gamma e^{+j\beta y}), \quad \text{for } 0 \le y \le L$$

and

$$I(y) = I_0(e^{-j\beta y} - \Gamma e^{+j\beta y}), \quad \text{for } 0 \le y \le L \tag{10}$$

where $I_0 = V_0/Z_c$ and β is the constant of propagation in the transmission line

$$\beta = k_0\sqrt{\epsilon_{\text{eff}}} \tag{11}$$

and Γ is the reflection coefficient at the end of the line:

$$\Gamma = \frac{R - Z_c}{R + Z_c}. \tag{12}$$

The time dependence $e^{j\omega t}$ is assumed but omitted everywhere in this work.

When $R = Z_c$ the line is matched and $\Gamma = 0$. Assuming that the current amplitude is constant across the line, one obtains that the surface current density in an end-fed line is

$$\bar{J}(x,y) = \hat{y}\frac{I_0}{W_l}e^{-j\beta y} \cdot \operatorname{rect}\left(\frac{x}{W_l}\right), \qquad \text{for } 0 \le y \le L \tag{13}$$

where

$$\operatorname{rect}\left(\frac{x}{W_l}\right) \equiv \begin{cases} 1, & \text{for } -W_l/2 \le x \le +W_l/2 \\ 0, & \text{elsewhere.} \end{cases}$$

For a center-fed line, which is matched at both ends, the surface current density is

$$\bar{J}(x,y) = \begin{cases} \hat{y}\left(\frac{I_0}{W_l}\right) \cdot e^{-j\beta y} \operatorname{rect}\left(\frac{x}{W_l}\right), \\ \qquad \text{for } 0 \le y \le L/2 \\ -\hat{y}\left(\frac{I_0}{W_l}\right) \cdot e^{+j\beta y} \operatorname{rect}\left(\frac{x}{W_l}\right), \\ \qquad \text{for } -L/2 \le y \le 0. \end{cases} \tag{14}$$

In order to calculate the radiation from these microstriplines the Fourier transforms of the surface currents should be used. For an end-fed line one gets

$$\tilde{\bar{J}}(k_x,k_y) = \hat{y}I_0\left(\frac{e^{+j(k_y-\beta)L} - 1}{j(k_y - \beta)}\right)\operatorname{sinc}\left(\frac{k_x W_l}{2}\right) \tag{15}$$

and for a center-fed line

$$\tilde{\bar{J}}(k_x,k_y) = \hat{y}I_0\left(\frac{e^{+j(k_y-\beta)L/2} - 1}{j(k_y - \beta)} - \frac{1 - e^{-j(k_y+\beta)L/2}}{j(k_y + \beta)}\right)\operatorname{sinc}\left(\frac{k_x W_l}{2}\right) \tag{16}$$

where $\operatorname{sinc}(x) \equiv \sin(x)/x$.

The radiated power is now calculated by substituting the relevant current distributions into (5). The surface waves are calculated by substituting these currents into (7). The input power to the microstripline is given by

$$P_{\text{in}} = \frac{1}{2}I_0^2 Z_c \tag{17}$$

so that for a current with an amplitude of 1 A the radiation *loss* and the surface wave *loss* are defined as

$$\frac{P_r}{P_{\text{in}}} = \frac{2P_r}{Z_c} \tag{18}$$

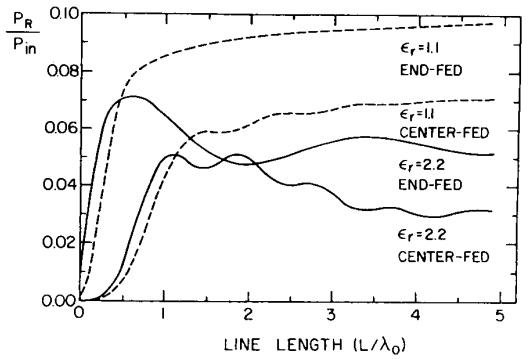

Fig. 2. Calculated free space radiation loss of a microstripline as a function of the line length. Four cases are studied: end-fed ($\epsilon_r = 1.1, 2.2$) and center-fed ($\epsilon_r = 1.1, 2.2$). Other parameters of the line are: characteristic impedance $Z_c = 100\ \Omega$ and thickness $h = 1.6$ mm. The frequency is $f = 10$ GHz.

and

$$\frac{P_s}{P_{\text{in}}} = \frac{2P_s}{Z_c}, \tag{19}$$

respectively.

A set of representative results has been derived using the above procedure. The radiation losses of typical end-fed and center-fed microstriplines with dielectric constants of $\epsilon_r = 1.1$ and 2.2 are shown in Fig. 2. The general conclusions concerning the losses in such lines are as follows.

- From (18) and (19) it follows that the losses are proportional to $1/Z_c$. The radiation power (P_r) and the surface wave excitation (P_s) are weakly dependent on Z_c so that the dependence of the losses on $1/Z_c$ is dominant. In general, the desire to minimize radiation and surface wave losses suggests that high characteristic impedance should be chosen.
- For a microstripline with given length and characteristic impedance, the radiation loss increases with $(h\sqrt{\epsilon_r}/\lambda_0)^2$ and the surface wave loss increases with $(h\sqrt{\epsilon_r}/\lambda_0)^3$. This is exact in the limits $h\sqrt{\epsilon_r}/\lambda_0 << 1$ and $\epsilon_r \to 1$, but is still a good approximation for standard dielectric substrates with $h\sqrt{\epsilon_r}/\lambda_0) \approx 0.1$ and $\epsilon_r \approx 2.2$. Thus, the desire to decrease radiation losses dictates low values of $h\sqrt{\epsilon_r}/\lambda_0$.
- For a microstripline with given thickness and characteristic impedance, the radiation loss depends on the line length as follows: in the range of $0 < L < \lambda_0$ the loss grows with $(L/\lambda_0)^2$. For the length greater than $L \gtrsim 3\lambda_0$ they are not sensitive to the length. The behavior of the surface wave loss as a function of the line length is oscillatory.
- The radiation losses are higher in end-fed microstrip lines than in center-fed lines. The reason is that a center-fed line carries two oppositely directed currents which tend to "cancel" each other. The surface wave losses are almost the same for end-fed and center-fed lines.
- Practical values for typical losses in microstriplines with $\epsilon_r = 2.2$, $h\sqrt{\epsilon_r}/\lambda_0 = 0.08$ and impedance of 200 Ω are about 3 percent (center-fed) to 5 percent (end-fed). These values are, as said, inversely proportional to the impedance, proportional to the square of the thickness, and not sensitive to the length.

The ohmic and dielectric losses are well known in the lit-

erature [13]–[15]. We consider only a nonmagnetic dielectric substrate in which the losses per unit length are small and can be calculated in terms of an attenuation factor α in the transmitted power $P(y)$:

$$P(y) = P_0 e^{-2\alpha y}. \tag{20}$$

Here y denotes a point along the direction of propagation (Fig. 1) and P_0 is the input power to the line at $y = 0$. The attenuation factor α is the sum of a dielectric factor α_d and an ohmic factor α_c:

$$\alpha = -\frac{dP/dy}{2P(y)} = \frac{P_c + P_d}{2p(y)} \quad \frac{\text{nepers}}{\text{unit length}} \tag{21}$$

or

$$\alpha_d = \frac{P_d}{2P(y)} \frac{\text{nepers}}{\text{unit length}}; \quad \alpha_c = \frac{P_c}{2P(y)} \frac{\text{nepers}}{\text{unit length}} \tag{22}$$

where P_d and P_c are the average dielectric and ohmic power losses per unit length, respectively. For the sake of convenience, the attenuation factor is given in dB/length units, thus the overall loss of the line is found by multiplying the attenuation factor by the length of the line. Several considerations for printed antennas should be pointed out. 1) The dielectric loss is not sensitive to the geometry of the line but it depends on the loss tangent, tan δ, of the material used. In common materials tan δ grows linearly with the frequency f. 2) The ohmic loss is high for narrow lines and for high impedances. It is also proportional to the skin resistance of the metal and thus goes up with $\sqrt{f}$. 3) The dissipation ohmic losses are therefore a technological factor, while the radiation and surface wave losses depend mainly on the line structure and can be minimized by appropriate design. 4) The dissipative losses increase linearly with the line length and thus play an important role in the efficiency of large arrays. It is interesting to notice that, once the substrate is chosen, the dissipation losses can be reduced by choosing feed lines with low impedances, but the radiation and surface wave losses would become higher. As a result, the total loss is not sensitive to the chosen impedances within the range of 100–200 Ω.

III. Four-Element Array Including Feed Network

In this section we describe the radiation and the surface wave excitation of a four-element array including its printed feed network. The printed layout and the relevant currents are shown in Fig. 3. The following results are presented: radiation patterns in the E- and H-planes, the radiation efficiency due to surface waves, the directivity, and the gain. Part of the results are shown also for the case where the feed network is omitted and some of the results are compared to experimental measurements.

The printed array includes four patches with distances D in both directions. Each patch has a length of L_p and a width of W_p. The patches are represented by four standing-wave currents I_p (put $\Gamma = 1$ in (12)), in a transmission-line with propagation constant β_p (derived by (8) and (11)) and characteristic impedance Z_c (9). The length of the patch is determined by the resonance condition: $\beta_p L_p = \pi/2$, and the width W_p is

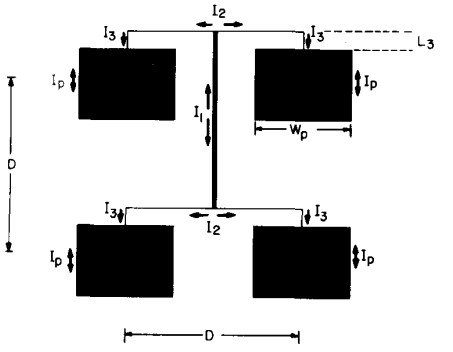

Fig. 3. Four element antenna geometry. The currents in the feed network are I_1, I_2, I_3. The currents in the patches are I_p. The distance between the patches is D in both directions. The length of the segments which enter the patches is L_3. Note that I_2 is x-directed and all the other currents are y-directed.

calculated iteratively as will be explained later on. The network includes a center line of 100 Ω fed at its center by an ideal 50 Ω source. In each one of the splitting points there are two 200 Ω lines going to the patches. The modeling of this network is done by traveling-wave currents I_1, I_2, I_3 following the approach described in the previous section. Notice that I_1 and I_2 are center-fed currents while I_3 is an end-fed current.

Fixing the relative amplitudes of the currents in the network and in the elements is an important point of this analysis. The basic assumption is that the supplied power is totally dissipated through free space radiation and surface waves. Hence, the resistance of each patch must be equal to the characteristic impedance Z_3. The procedure is the following: first, we normalize the amplitude of I_1 to be 1 A and the phase in the central feed point as zero. This choice determines all the amplitudes and phases in the feed network in such a way that the propagating power along the lines is conserved and the phase is continuous. Secondly we choose a value for W_p and use the condition of continuity of the voltages:

$$I_p Z_p = I_3 Z_3 e^{-j(\beta_3 L_3 + \pi/2)} \tag{23}$$

to find the amplitude of I_p. Then the radiation resistance R_r and surface wave resistance R_s are calculated and their sum is compared to Z_3. The width of the patch W_p is then changed iteratively until

$$R_r + R_s = Z_3. \tag{24}$$

The ratio between the current I_p and the current I_3 presents the quality factor Q of the radiating elements. It should be noted again that the above currents and the associated radiation properties are based on the approximation that the element is an ideal resonator or a section of an ideal transmission-line. From these currents one gets the radiated power, the surface wave power, and their equivalent real resistance. This resistance is then added to the feed network providing a match. The discussion on the validity ranges of this method is beyond the scope of this work. However, for high-Q microstrip elements it is a useful tool [20]. It is clear also that the approximation is good for the *feed lines,* whose radiation is much smaller than their input power (3–5 percent).

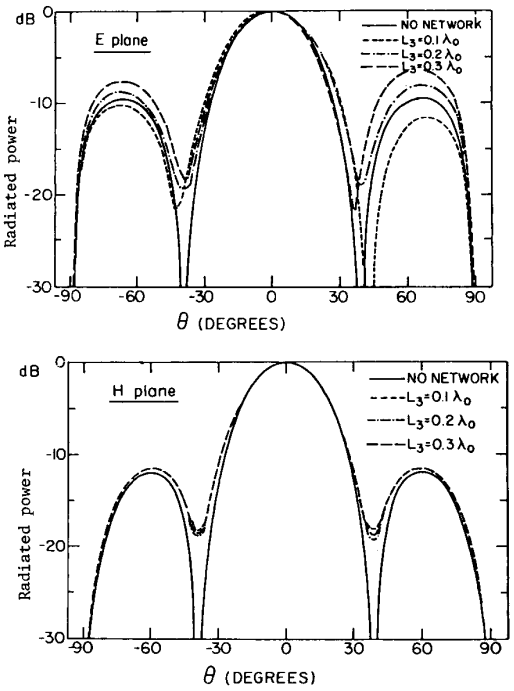

Fig. 4. Calculated radiation patterns of a four element array. The dielectric constant is $\epsilon_r = 2.2$, the thickness is $h\sqrt{\epsilon_r}/\lambda_0 = 0.08$, and the spacing is $D/\lambda_0 = 0.8$. Results are given for three values of L_3/λ_0 and for an array without the network. (a) For E-plane. (b) For H-plane.

A set of representative radiation patterns of this four element array is shown in Fig. 4. The results are shown for different values of the section length L_3. Although for practical design purposes one usually takes L_3/λ_0 to be small, it was found to be a suitable parameter for checking the analysis. The effects of the feed network on the sidelobes are significant in the E-plane pattern. The influence on the H-plane is less important due to the orthogonality of I_2 and the symmetry of all the other currents in this cut. Calculated results are shown also for an array without the feed network.

The radiation efficiency due to surface waves is defined as the ratio between the radiated power and the total power of radiation and surface waves:

$$\eta_s \equiv \frac{P_r}{P_r + P_s}. \tag{25}$$

Fig. 5 shows the calculated surface wave efficiency as a function of the spacing between close patches for three values of $h\sqrt{\epsilon_r}/\lambda_0$ and for a fixed value of L_3. Results without the feed network are also shown. The efficiency decreases as D/λ_0 increases and this effect is related to the strong interference between surface waves excited by co-linear elements on the $\hat{y}$ axes (7). The surface wave loss has a minimum when $D \approx \lambda_0/2$ and a maximum when $D \approx \lambda_0$. The gain is calculated by

$$G = D_{ir} - \eta, \quad \text{dB} \tag{26}$$

where η is the power efficiency of the antenna:

$$\eta = \eta_s + \eta_d + \eta_c + \eta_{cr}, \quad \text{dB} \tag{27}$$

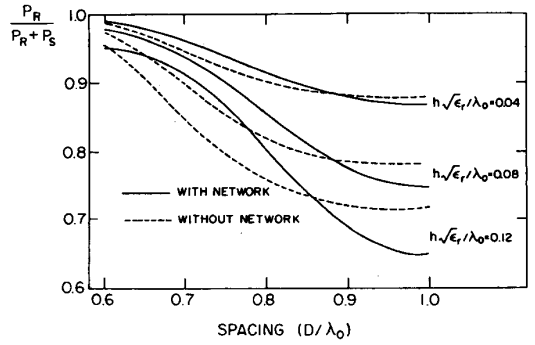

Fig. 5. Calculated efficiency due to surface wave losses of a four element array. P_r is the free space radiated power and P_s is the power radiated by surface waves. The segment $L_3/\lambda_0 = 0.1$, and the dielectric constant is $\epsilon_r = 2.2$. Results are given for three values of $h\sqrt{\epsilon_r}/\lambda_0$, with and without the network.

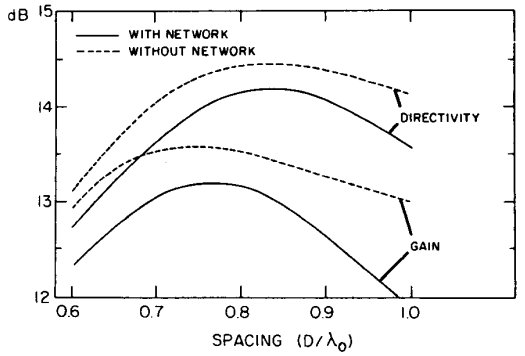

Fig. 6. Calculated directivity and gain of four-element arrays. The dielectric constant is $\epsilon_r = 2.2$, the thickness is $h\sqrt{\epsilon_r}/\lambda_0 = 0.08$ and $L_3/\lambda_0 = 0.1$.

and η_d and η_c are the efficiencies due to dielectric and ohmic losses. The efficiency due to connector losses η_{cr} is estimated theoretically [20] and checked experimentally [21] to be lower than 0.2 dB the mentioned substrate parameters. Fig. 6 shows the calculated directivity and gain as a function of D/λ_0 where $L_3/\lambda_0 = 0.1$ and $h\sqrt{\epsilon_r}/\lambda_0 = 0.08$. The directivity is calculated according to the definition:

$$D_{ir} = \frac{4\pi f(\theta, \phi)_{\max}}{P_r} \tag{28}$$

where $f(\theta, \phi)_{\max}$ denotes the maximum radiation intensity. Results without the feed network are again given for comparison. Maximum directivity and maximum gain occur for different values of D/λ_0 (0.83 and 0.76, respectively). The ohmic and dielectric losses are calculated to be 0.14 dB at 10 GHz. The difference between the directivity and the gain is caused mainly by surface wave losses.

A set of seven four-element arrays with different lengths L_3 had been built and tested. The antennas were designed to work at a resonance frequency of 10 GHz and the dielectric substrate was OAK-605, which has $\epsilon_r = 2.2$ and $h = 1.6$ mm ($h\sqrt{\epsilon_r}/\lambda_0 = 0.08$). The spacing between close elements was $D = 24$ mm ($0.8\ \lambda_0$) and the line widths were $W_1 = 1.5$ mm ($Z_1 = 98\ \Omega$) and $W_2 = W_3 = 0.2$ mm ($Z_2 = Z_3 = 193\ \Omega$). The width and length of the patches were chosen empirically

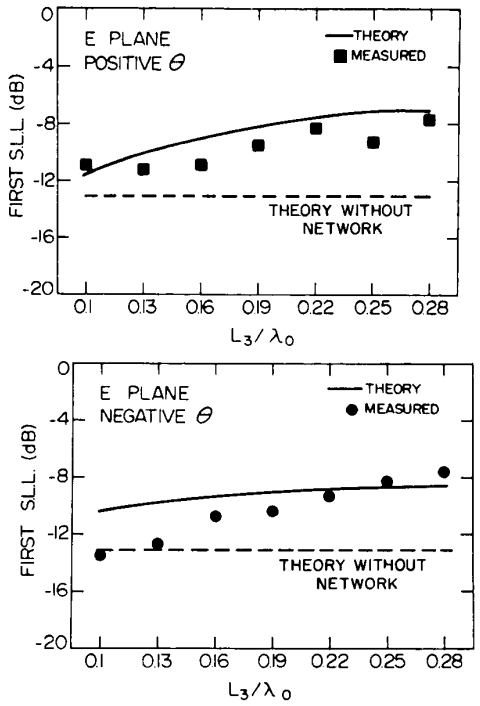

Fig. 7. The first sidelobe levels in the E plane for seven four-element arrays with different values of L_3/λ_0. (a) Positive Θ. (b) Negative Θ.

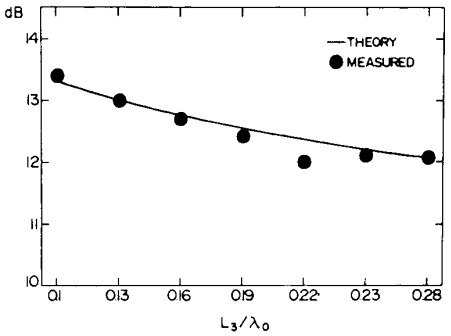

Fig. 8. The gains of four-element arrays with different values of the segment length L_3/λ_0. The spacing between close elements is $D/\lambda_0 = 0.8$.

TABLE I
CALCULATED DIRECTIVITY, LOSSES AND GAIN AND THE MEASURED GAIN (ALL IN dB) FOR A SET OF FOUR-ELEMENT ANTENNA ARRAYS WITH SEVEN VALUES OF THE SEGMENT L_3 (SEE FIG. 10)

L_3/λ_0	0.1	0.13	0.16	0.19	0.22	0.25	0.28
directivity without network	14.4	14.4	14.4	14.4	14.4	14.4	14.4
radiation loss	0.2	0.3	0.4	0.5	0.6	0.7	0.7
surface-wave loss	0.6	0.8	0.9	1.0	1.1	1.2	1.3
dielectric and ohmic losses	0.1	0.1	0.1	0.1	0.1	0.1	0.1
connector loss	0.2	0.2	0.2	0.2	0.2	0.2	0.2
calculated GAIN	13.3	13.0	12.8	12.6	12.4	12.2	12.1
measured GAIN	13.3	13.0	12.7	12.4	12.0	12.1	12.1

to match a central frequency of 10 GHz: $W_p = 8.9$ mm and $L_p = 11.2$ mm. It is interesting to compare these values with the values obtained by the iteration suggested before: $W_p = 9.4$ mm and $L_p = 10.2$ mm. The lengths of the last line segments were $L_3/\lambda_0 = 0.1, 0.13, 0.16, 0.19, 0.22, 0.25$, and 0.28. The measured resonance frequency was 9.9 GHz for all the measured antennas, but similar results were obtained at near-resonance frequencies of 9.8 and 10.0 GHz. Gain and pattern measurements were made outdoors at a distance of 25 m.

Fig. 7 shows measured and calculated sidelobe levels (SLL) in the E-plane as a function of L_3, both for positive and negative θ. An additional graph (the dashed line) shows the SLL of a four-element array without the feed network. The evaluation of the accuracy of the measurements is difficult. However, good reproducibility was obtained in many sets of measurements, including the inversion of the antenna direction in both the E- and H-planes. The SLL in the H-plane do not change with L_3, as expected from the theory, but in the E-plane we find an obvious tendency of the SLL to increase with L_3/λ_0. The measured and calculated gain as a function of L_3 are shown in Fig. 8. The accuracy of these measurements is better than 0.5 dB and the agreement of the measurement results with the theory is good. The dependence of the gain on L_3 is mainly caused by the increase in the surface wave loss, as can be seen from the loss budget in Table I.

The agreement between the measured and calculated results is better for the gain than for the sidelobes. We conclude that the main reason for the difference between the theory and the measurements is connected with the approximations made in the described model. The surface currents in the antenna are not self-consistently solved, and corrections due to the mutual interaction between the currents are not calculated. The effects of the vertical feed and the effects of the finite ground plane are also ignored. The accuracy of the current model is therefore limited, and seems to be better for integral quantities, like the gain. However, the overall behavior of the radiation patterns fits the measured results better than a simpler model that neglects the feed network.

IV. Directivity and Gain in Large Arrays

The effects of the feed network become important in high gain miscostrip array antennas with large numbers of radiating elements and complicated feed networks. It is the purpose of this section to present results of the gain limitations in large modular arrays. Consider $n \times n$ microstrip arrays where $n = 2, 4, 8, 16, \cdots$ with single layer power dividing network. Fig. 9 shows the layouts of 16, 64, and 256 element arrays built in such a way [16], [17]. The two basic building blocks are the four-element array (but with a center line of 200 Ω) and an "H" shaped feed network. The four-element subarray is changed a little in the layout shown in Fig. 3. The central line has been moved down and small diagonal sections have been inserted as can be seen in Fig. 9. This change was made in order to permit the connection of the "H" network to the center of the four-element subarray. The sensitivity of the directivity and the gain results to this change were checked and found negligible. The 16-element array is constructed from

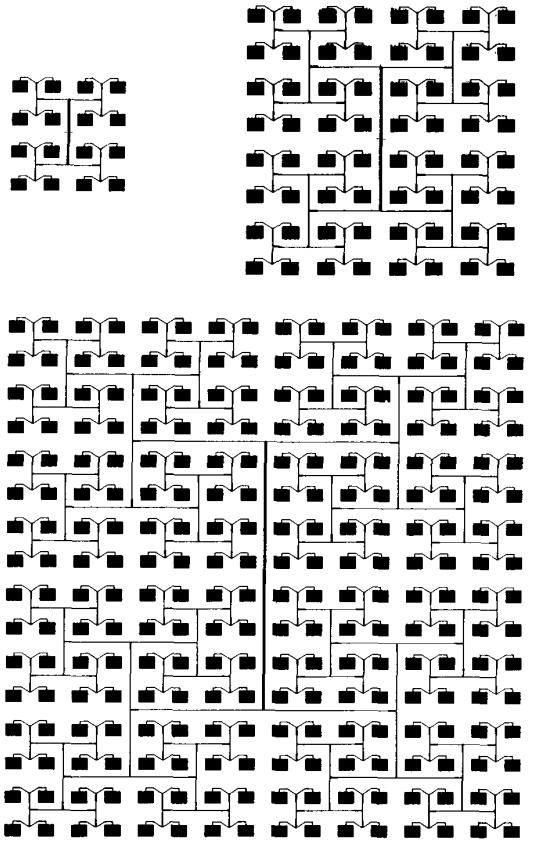

Fig. 9. Layouts of modular arrays of 16, 64, and 256 elements.

four subarrays connected and fed by the "H" network. The 64-element array is constructed again from four subarrays of 16 elements each and another "H" network, and so forth. In each one of the "H" networks there are several quarter wavelength transformers for matching. The current in each transformer is represented by two oppositely directed waves. Their amplitudes are determined by continuity of the voltages at the ends and conservation of the power.

The calculation of the radiation properties of these arrays is done easily by multiplying the building blocks with the appropriate array factors.

In addition to the radiation and the surface wave losses, the dissipative losses are derived by the multiplication of the electrical path length of the lines by the attenuation factor. The dissipative losses of the radiating elements are small but are also taken into account according to [15]. A detailed loss budget of a set of modular arrays with typical parameters is given in Table II. A comparison is made with the gain of a reflector antenna having the same area and an aperture efficiency of 50 percent. It can be seen that arrays of up to 1024 elements are predicted to have about the same gain as a reflector but larger printed arrays are not practical where reasonable efficiency is needed. It also can be seen that the dielectric and ohmic losses become dominant in these high gain arrays, and novel feeding techniques should be considered. Fig. 10 shows the calculated gain and the directivity as a function of the spacing between close elements D/λ_0. The dielectric, constant is

TABLE II
A DETAILED CALCULATED LOSS BUDGET OF MODULAR MICROSTRIP ARRAYS AT 10 GHz, DIELECTRIC CONSTANT IS $\epsilon_r = 2.2$, THICKNESS IS $h = 1.6$ mm, AND SPACING BETWEEN CLOSE ELEMENTS $0.8\lambda_0$; ALL NUMBERS ARE GIVEN IN dB

number of elements	16	64	256	1024	4096
directivity without network	20.9	27.0	33.0	39.2	45.1
radiation loss	0.8	1.0	1.3	1.9	2.6
surface wave loss	0.3	0.3	0.2	0.2	0.1
dielectric loss	0.1	0.3	0.5	1.0	2.1
ohmic loss	0.1	0.3	0.6	1.2	2.4
connetor loss	0.2	0.2	0.2	0.2	0.2
calculated gain	19.5	25	30	34.5	37.5
gain of a dish	18	24	30	36	42

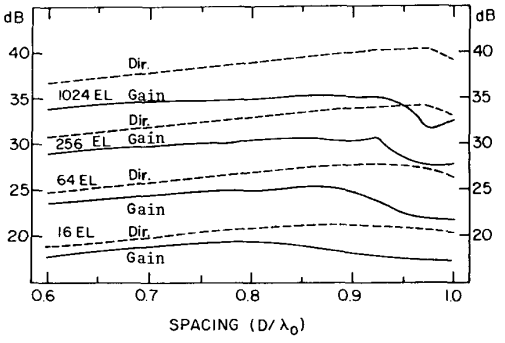

Fig. 10. Calculated directivity and gain of microstrip arrays with 16, 64, 256 and 1024 elements as a function of the spacing between close elements D/λ_0. The dielectric constant is 2.2, the thickness is $h\sqrt{\epsilon_r}/\lambda_0 = 0.08$, and the frequency is $f = 10$ GHz.

2.2, the thickness is 1.6 mm, and the frequency is 10 GHz. It can be seen that the directivity increases with D/λ_0 and a maximum is reached in the range of 0.8–0.9 λ_0. The gain is less sensitive to the spacing because the ohmic, dielectric and surface wave losses increase with the spacing. One can see that, for values of D greater than 0.9 λ_0, the surface wave loss increases rapidly. The results reported here agree quite well with the results of Hall and Prior [11]. For example, the estimated losses given there, at 12 GHz for a substrate with a thickness of 1.6 mm and a dielectric constant of 2.32, are higher than our estimated results by 0.3, 0.8, 1.3, 1.7, and 1.8 dB for the arrays of 16, 64, 256, 1024 and 4096 elements, respectively. The difference is mainly the result of the higher frequency and the higher dielectric constant. An adaptation of these parameters in our analysis shows that both estimates agree within 1 dB.

A set of 16, 64, 256, and 1024 element arrays was built and tested at frequencies of 10, 20, 30, and 35 GHz (except for the 1024 element array at 10 GHz whose dimensions are 80 × 80 cm). All the antennas were built on the same material (OAK-605 or Duroid 5880) with accurate scaling in all the relevant dimensions. The spacing was 0.8 λ_0 in all cases. The photoresist coating and the etching process were done in homemade facilities with excellent accuracies. The

TABLE III
CALCULATED AND MEASURED GAINS OF MICROSTRIP ARRAY ANTENNAS (IN dB); DIELECTRIC CONSTANT $\epsilon_r = 2.2$, THICKNESS $h\sqrt{\epsilon_r}/\lambda_0 = 0.08$ AND SPACING BETWEEN CLOSE ELEMENTS $D/\lambda_0 = 0.8$

No. of elements	16	64	256	1024
10 GHz				
calculated gain	19.2	24.8	30.3	34.9
measured gain	19.5	25.0	29.5	—
20 GHz				
calculated gain	19.1	24.7	29.9	34.2
measured gain	19.8	24.5	29.7	34.1
30 GHz				
calculated gain	19.0	24.5	29.6	33.5
measured gain	19.5	24.0	28.5	32.0
35 GHz				
calculated gain	19.0	24.4	29.4	33.2
measured gain	19.0	24.0	28.5	32.0

thin feed lines in the higher frequencies have a width of 70 ± 10 micron without any detected cuts. The comparison between calculated and measured results is given in Table III. The radiation and surface wave losses for a given number of elements are identical at all four frequencies and appear in Table II. The difference between the gains at different frequencies is the result of the growing dissipation losses. The agreement between calculated and measured results is in general very good. An independent efficiency measurement of these antennas which was made by a radiometric method [23] gave consistent results for the losses within an accuracy of 0.5 dB.

V. Conclusion

An analytical approach for the analysis of microstrip arrays including their feed network is introduced. This approach is based on an educated guess of the currents in the radiating elements and in the feed lines. It is a useful tool for high Q-radiators and for quasi-TEM transmission lines. Modular structures of feed networks are handled in a simple and efficient way using closed-form expressions.

Calculated results of radiation patterns, directivity, and gain of a four element array are shown and the experimental results show reasonable agreement with the theory.

The analysis has been extended to large modular arrays and a detailed loss budget for a typical set of parameters proves that single-layer arrays with up to 1024 elements have about the same gain as reflectors having the same area. The experimental results for a set of 16, 64, 256 and 1024 element arrays agree very well with the theoretical prediction.

References

[1] J. R. James, P. S. Hall, and C. Wood, *Microstrip Antenna Theory and Design*. London: Peter Peregrinus, 1981, ch. 5, 6.

[2] R. J. Mailloux, J. F. McIlvenna, and N. P. Kernweis, "Microstrip array technology," *IEEE Trans. Antennas Propagat.*, vol. AP-29, pp. 25–37, Jan. 1981.

[3] M. A. Weiss, "Microstrip antennas for millimeter waves," *IEEE Trans. Antennas Propagat.*, vol. AP-29, pp. 171–174, Jan. 1981.

[4] S. Nishimura, Y. Sugio, and T. Makimoto, "Cranck-type circularly polarized microstrip line antenna," in *IEEE Antennas Propagat. Soc. Int. Symp. Dig.*, 1983, pp. 162–165.

[5] M. Ando, K. Sakurai, N. Goto, K. Arimura, and Y. Ito, "A radial line slot antenna for 12 GHz satellite TV reception," *IEEE Trans. Antennas Propagat.*, vol. AP-33, pp. 1347–1353, Dec. 1985.

[6] E. Rammos, "A new wideband high gain suspended substrate line planar array for 12 GHz satellite TV," in *Proc. 13th European Microwave Conf.* 1983, pp. 227–231.

[7] G. Dubost and C. Vinatier, "Large bandwidth and high gain array of flat folded dipoles acting at 12 GHz," in *Proc. IEE ICAP,* 1983, pp. 145–149.

[8] A. Henderson and J. R. James, "Improved microstrip flat plate array for domestic DBS reception," in *IEEE Antennas Propagat. Soc. Int. Symp. Dig.*, 1986, pp. 565–568.

[9] E. H. Newman and J. E. Tehan, "Analysis of a microstrip array and feed network," *IEEE Trans. Antennas Propagat.*, vol. AP-33, pp. 397–403, Apr. 1985.

[10] S. M. Voda and D. M. Pozar, "A rigorous analysis of a microstrip line fed patch antenna," in *IEEE Antenna Propagat. Soc. Int. Symp. Dig.*, 1986, pp. 825–828.

[11] P. S. Hall and C. J. Prior, "Radiation control in corporately fed microstrip patch arrays," in *JINA '86 Dig.*, Nice, 1986, pp. 271–275.

[12] P. Perlmutter, S. Shtrikman, and D. Treves, "Electric surface current model for the analysis of microstrip antennas with application to rectangular elements," *IEEE Trans. Antennas Propagat.*, vol. AP-33, pp. 301–311, Mar. 1985.

[13] R. A. Pucel, D. J. Masse, and C. P. Hartwig, "Losses in microstrip," *IEEE Trans. Microwave Theory Tech.*, vol. MTT-16, pp. 342–350, June 1968, p. 1064, Dec. 1968.

[14] E. J. Denlinger, "Losses of microstrip lines," *IEEE Trans. Microwave Theory Tech.*, vol. MTT-28, pp. 513–522, June 1980.

[15] W. F. Richards, Y. T. Lo, and J. Brewer, "A simple experimental method for separating loss parameters of a microstrip antenna," *IEEE Trans. Antennas Propagat.*, vol. AP-29, pp. 150–151, Jan. 1981.

[16] J. Ashkenazy, P. Perlmutter, and D. Treves, "A modular approach for the design of microstrip antennas," *IEEE Trans. Antennas Propagat.*, vol. AP-31, pp. 190–193, Jan. 1983.

[17] E. Levine, G. Malamud, and D. Treves, "High gain modular microstrip antennas," in *Proc. 16th European Microwave Conf.*, 1986, pp. 655–660.

[18] M. V. Schneider, "Microstrip lines for microwave integrated circuits," *Bell Syst. Tech. J.*, vol. 48, pp. 1422–1444, 1969.

[19] R. E. Collin, *Foundations for Microwave Engineering*. New York: McGraw-Hill, 1966, ch. 3.

[20] W. F. Richards, Y. T. Lo, and D. D. Harrison, "An improved theory for microstrip antennas and applications," *IEEE Trans. Antennas Propagat.*, vol. AP-29, pp. 38–46, Jan. 1981.

[21] S. Pinhas and S. Shtrikman, "Vertical currents in microstrip antennas," *IEEE Trans. Antennas Propagat.*, vol. AP-35, pp. 1285–1289, Nov. 1987.

[22] E. Levine and D. Treves, "Test technique improves coax-to-microstrip transmissions," *Microwaves,* vol. 25, pp. 99–102, July 1986.

[23] J. Ashkenazy, E. Levine, and D. Treves, "Radiometric measurement of antenna efficiency," *Electron. Lett.*, vol. 21, pp. 111–112, Jan. 1985.

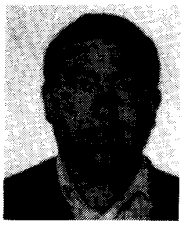

Ely Levine (S'84–M'86) was born in Tel Aviv, Israel, on September 30, 1952. He received B.S.E.E. and M.S.E.E. degrees from the Technion–The Israeli Institute of Technology in 1978 and 1981, respectively, and a Ph.D. degree in applied physics from the Weizmann Institute of Science, Rehovot, Israel in 1987.

From 1978 to 1982 and in 1987 he served as a research engineer in the Electronics Department of the Weizmann Institute. In 1986 he spent several months as a guest scientist at the FGAN (Establishment for Applied Sciences) in Wachtberg-Werthhoven, West Germany. In July 1987 he joined the Antenna Department at Elta Electronics Industries, Ashdod, Israel. His experience includes: dielectric measurements of radomes,

special measurement techniques in microwaves and antennas, development of practical printed antennas and studies on theoretical and experimental aspects of printed antennas. He is the Vice-Chairman of the IEEE AP/MTT Joint Chapter in Israel.

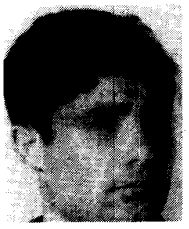

Gabi Malamud was born in Argentina on October 25, 1958. He received the B.Sc. degree in physics from Ben Gurion University, Beer Sheva, Israel in 1983, and the M.Sc. degree in applied physics from the Weizmann Institute of Science in 1986.

He is currently a Ph.D. student in the Weizmann Institute of Science, Rehovot, Israel, and his research interest is in particle detectors.

Shmuel Shtrikman (M'59–F'73) for a photograph and biography please see page 300 of the March 1985 issue of this TRANSACTIONS.

David Treves (SM'69–F'76) for a photograph and biography please see page 300 of the March 1985 issue of this TRANSACTIONS.